Available online at www.sciencedirect.com
ScienceDirect
Journal of the European Ceramic Society 29 (2009) 787–794
www.elsevier.com/locate/jeurceramsoc

Mechanical behavior of two-step hot-pressed ZrB_2-based composites with $ZrSi_2$

Shu-Qi Guo [a,*], Yutaka Kagawa [a,b], Toshiyuki Nishimura [c]

[a] *Composites and Coatings Center, National Institute for Materials Science, 1-2-1 Sengen, Tsukuba, Ibaraki 305-0047, Japan*
[b] *Research Center for Advanced Science and Technology, The University of Tokyo, 4-6-1 Komaba, Meguro-ku, Tokyo 153-8505, Japan*
[c] *Nano Ceramic Center, National Institute for Materials Science, 1-1 Namiki, Tsukuba, Ibaraki 305-0044, Japan*

Received 29 March 2008; received in revised form 12 June 2008; accepted 20 June 2008
Available online 19 August 2008

Abstract

In this study, fully dense ZrB_2-based composites containing $ZrSi_2$ were sintered using a two-step hot pressing process. The elastic moduli, fracture toughness and flexural strength of the hot-pressed composites were determined. The effects of $ZrSi_2$ content on densification behavior and properties of the composites were assessed. The results indicated that the $ZrSi_2$ improved the sinterability of ZrB_2 powders. Fully dense ZrB_2-based composites with $ZrSi_2$ were obtained at 1550 °C for 20–40 vol.% $ZrSi_2$-conatining ZrB_2 powders. The microstructure of the resulting composites was fine and homogeneous. The elastic moduli, fracture toughness and flexural strength of the obtained composites depended on $ZrSi_2$ content. The shear, Young's, and bulk moduli decreased with $ZrSi_2$ content. The range of fracture toughness values was measured to be 3.8–4.8 MPa $m^{1/2}$. The flexural strength, which was 556 MPa, was almost the constant for $ZrSi_2$ content of 30 vol.% or less. For 40 vol.% $ZrSi_2$, however, the strength lowered significantly to 382 MPa.

Keywords: ZrB2; ZrSi2; Densification; Microstructure; Mechanical properteis

1. Introduction

Zirconium diborides (ZrB_2)-based composites have an extremely high-melting point (>3000 °C), high-thermal and -electrical conductivities, chemical inertness against molten metals, and good thermal shock resistance.[1,2] These unique mechanical and physical properties have never been achieved by other ceramics materials, e.g., Al_2O_3, ZrO_2, Si_3N_4, and SiC. Recently, the ZrB_2-based ceramics composites are being considered for use as potential candidates for a variety of high-temperature structural applications, including furnace elements, plasma-arc electrodes, or rocket engines and thermal protection structures for leading-edge parts on hypersonic re-entry space vehicles at over 1800 °C.[1–5]

However, it is very difficult to obtain fully dense ZrB_2 ceramics because the densification of ZrB_2 powders generally requires very high temperatures (>2100 °C),[6] owing to the high-melting point and low-self-diffusivity. To improve sinterability, nitrides, like AlN, Si_3N_4, ZrN, are added to pure ZrB_2,[7–9] producing an intergranular secondary phase that aids the densification of ZrB_2. This makes densification of ZrB_2 powders at a lower temperature of 1900 °C possible. In addition, the disilicides of transition metals are another alternative additive because these disilicides improve sinterability as well as increase oxidation resistance of ZrB_2 ceramics. Recently, the ZrB_2-based ceramics with $MoSi_2$ additive were sintered by pressureless and/or by hot press at a temperature below 1850 °C.[10–13] The resulting composites showed high-flexural strength,[10,11] good oxidation resistance,[12] high-thermal and -electrical conductivities.[13] This shows that the disilicides of the transition metals are a potential additive for lowering sintering temperature of the ZrB_2-based ceramics. Furthermore, it is possible to further lower sintering temperature of ZrB_2-based ceramics by selecting appropriate disilicides of transition metals. Thus, it is required for sintering ZrB_2-based composites at a lower temperature to explore a new additive of disilicides of the transition metal.

$ZrSi_2$ is one of refractory disilicides of the fourth group of transition metals, which has a low density, high-creep strength, and superior oxidation and is a very attractive material for application temperatures up to 1300 °C. Presumably, $ZrSi_2$ forms a

* Corresponding author. Tel.: +81 29 859 2223; fax: +81 29 859 2401.
E-mail address: GUO.Shuqi@nims.go.jp (S.-Q. Guo).

0955-2219/$ – see front matter © 2008 Elsevier Ltd. All rights reserved.
doi:10.1016/j.jeurceramsoc.2008.06.037

surface layer of silica due to surface oxidation of the powder particles during production and handling. The presence of silica can help the densification and act as a protective barrier against high-temperature oxidation of ZrB_2, which is similar to $MoSi_2$ powder particles.[11–13] In addition, the melting point of $ZrSi_2$ is ~1620 °C,[14] and it is lower than that of $MoSi_2$ (~2030 °C).[15] As a result, $ZrSi_2$ is a potential candidate additive for lowering sintering temperature of ZrB_2 instead of $MoSi_2$ additive.

On the other hand, two-step hot pressing is a promising approach to obtain fully dense carbide and boride ceramics with fine and homogeneous microstructure. The two-step sintering process consists of a first stage at lower temperature for longer time and a second one at higher temperature for short time. This advantage of such a cycle is that most of the densification occurs at a rather low temperature and that the higher temperature stage is short, subsequently, resulting in a fine and homogeneous microstructure. This was demonstrated in the ternary system TiB_2–TiC–SiC.[16] However, the two-step hot sintering process of ZrB_2-based composites and its effects on properties are not experimentally investigated yet. In the present study, the ZrB_2-based composites with $ZrSi_2$ were hot pressed by a two-step hot sintering at 1400 and 1550 °C, respectively, for a corresponding holding time of 30 and 15 min, under a pressure of 30 MPa in argon atmosphere. The elastic moduli of the resulting composites were calculated using the measured longitudinal and transverse soundwave velocities. The fracture toughness of the composites was determined using an indentation technique. The fracture strength of the composites was determined by fracture at room temperature, using four-point flexural. Also, the effects of $ZrSi_2$ content on the densification behavior and the mechanical properties were examined.

2. Experimental procedure

2.1. Starting powder

Commercially available ZrB_2 and $ZrSi_2$ powders produced by Japan New Metals Co. Ltd. (Grade F, Tokyo) were used in this study. The particle sizes of the ZrB_2 powder are in the range of 1.5–2.5 μm, an average grain diameter of 2.1 μm. The elemental impurities are (wt.%): O 1.06, C 0.27, and N 0.19. The particle sizes of the $ZrSi_2$ powder are in the range of 2.0–5.0 μm, average particle size ≈2.5 μm. The elemental impurities are (wt.%): O 0.73, C 0.10, and Fe 0.10. In order to examine the effect of $ZrSi_2$ content on the densification and mechanical properties, five batches of ZrB_2–$ZrSi_2$ compositions were prepared in this study. One is single-phase ZrB_2 and others contain 10, 20, 30, or 40 vol.% $ZrSi_2$. Hereafter, the five series of ZrB_2–$ZrSi_2$ compositions compacts are denoted as ZSZ0, ZSZ10, ZSZ20, ZSZ30, and ZSZ40, respectively. The detailed compositions are shown in Table 1. The powder mixtures were ball-milled using SiC milling media and ethanol under 160 rpm for 24 h, and the resulting slurries were then dried under magnetic stirring to avoid sedimentation. Before sintering, the dried mixtures were sieved through a metallic sieve with −60-mesh screen size.

2.2. Two-step hot sintering process

The obtained powder mixtures were then hot pressed (FVHP-1-3, Fuji Electric Co. Ltd., Tokyo, Japan) in graphite dies under 30 MPa in argon atmosphere in tablets averaging 21 mm × 25 mm × 3.5 mm in size. The temperature of the sample was monitored by a two-color optical pyrometer through a hole opened in the die. A two-step sintering process was used to obtain the fine and homogeneous microstructure. First, the powder compacts were heated to 1400 °C with a heating rate of 30 °C/min under a pressure of 30 MPa in argon atmosphere. After the hot press was held at 1400 °C for 30 min, the temperature was increased to 1550 °C with a heating rate of 25 °C/min, and then held for 15 min. The load was removed when the die temperature dropped below 1300 °C. Note the single-phase ZrB_2 powder (ZSZ0) was hot pressed at 2000 °C for holding time of 60 min under a pressure of 30 MPa. In addition, in order to compare the effect of two-step sintering process, one composition (ZSZ20) was hot pressed at 1550 °C for 30 min without the intermediate step at 1400 °C. The densities, ρ, of the sintered composite compacts were measured from Archimedes method with distilled water as medium. X-ray diffraction (XRD) was used for crystalline phase identification of the composites. Microstructure of the resulting ZrB_2–$ZrSi_2$ composites was characterized by field emission scanning electron microscopy (FE-SEM) and energy dispersive X-ray spectroscopy (EDX). The grain size, d, was determined by measuring the average linear intercept length, d_m, of the grains in FE-SEM images of sintered ZrB_2 ceramics, according to the relationship of $d = 1.56d_m$ which was given by Mendelson.[17]

Table 1
Compositions, true densities, relative densities and grain size of the various hot-pressed ZrB_2–$ZrSi_2$ composites

Materials	Compositions (vol.%)		Processing conditions	True density (g/cm^3)	Measured density (g/cm^3)	Relative density (%TD)	Grain size (μm)	
	ZrB_2	$ZrSi_2$					ZrB_2	$ZrSi_2$
ZSZ0	100	0	2000 °C/60 min/30 MPa	6.09	5.51	90.4	6.1 ± 2.7	
ZSZ10	90	10	1400 °C/30 min/30 MPa + 1550/15 min/30 MPa	5.97	5.77	96.6	2.3 ± 0.9	0.6 ± 0.4
ZSZ20	80	20	1400 °C/30 min/30 MPa + 1550/15 min/30 MPa	5.85	5.80	99.1	2.5 ± 0.8	0.7 ± 0.6
ZSZ30	70	30	1400 °C/30 min/30 MPa + 1550/15 min/30 MPa	5.73	5.72	99.8	2.6 ± 1.1	0.7 ± 0.6
ZSZ40	60	40	1400 °C/30 min/30 MPa + 1550/15 min/30 MPa	5.61	5.56	99.2	2.7 ± 1.0	0.9 ± 0.7
ZSZ20	80	20	1550/30 min/30 MPa	5.85	5.84	99.8	4.1 ± 1.5	0.7 ± 0.5

2.3. Characterization

The elastic moduli measurements of the composites were determined using ultrasonic equipment (TDS 3052B, Tektronix Inc., Beaverton, OR, USA) with a fundamental frequency of 20 MHz. The shear modulus, G, Young's modulus, E, bulk modulus, B, and Poisson's ratio, ν, were calculated using the longitudinal and transverse soundwave velocities measured in the composite specimens. The details of calculations were reported elsewhere.[18] The fracture toughness of the composites was determined using an indentation technique. The indentation tests were performed on the polished surface of the specimens by loading with a Vickers microhardness indenter (AVK-A, Akashi Co. Ltd., Yokohama, Japan) for 15 s in ambient air at room temperature. The corresponding diagonals of the indentation and crack sizes were measured using an optical microscope attached to the indenter. The indentation load of 49 N was used, and 10 indents were made for each measurement. The fracture toughness was calculated from the Anstis equation.[19] In addition, the ZrB_2–$ZrSi_2$ plates were cut into flexural bars with dimensions of ~25 mm × 2.5 mm × 2 mm. The surfaces of the specimen were ground with a 800-grit diamond wheel and the tensile surface was polished by diamond paste down to 1.0 μm. The edges of the specimen were then chamfered at 45°. The room temperature flexural strength of the composites was determined by fracture using four-point flexure (inner span 10 mm, outer span 20 mm). The bend test was performed using a testing system (Autograph Model AG-50KNI, Shimadzu Co. Ltd., Kyoto, Japan) with a crosshead speed of 0.5 mm/min. At least five specimens were used for each measurement. After the bend testing, the fracture surfaces of the specimens were examined by FE-SEM.

3. Results and discussion

3.1. Densification

In Fig. 1, typical examples of the shrinkage curves obtained during hot-pressing cycle for the various hot-pressed ZrB_2–$ZrSi_2$ composites are presented. For the single-phase ZrB_2 powder (Fig. 1(a)), the onset temperature of densification was at ~1780 °C which was ~500 °C higher than that of ZSZ10 powder. Only the density of ~91% was obtained even at 2000 °C for holding time of 60 min under a pressure of 30 MPa. On contrary, for the ZrB_2 powders containing $ZrSi_2$, the curves consist of two stages: a first stage at 1400 °C for 30 min and a second one at 1550 °C for 15 min (Fig. 1(b)). It is found that the onset temperature of densification lowered with increasing $ZrSi_2$ content: ~1280 °C for ZSZ10 powder, ~1260 °C for ZSZ20 powder, ~1240 °C for ZSZ30 powder, and ~1180 °C for ZSZ40 powder. This finding indicated that $ZrSi_2$ lowered the onset temperature of densification and this effect enhanced with $ZrSi_2$ content. In particular, for $ZrSi_2$ content of 40 vol.% (ZSZ40), the onset temperature of densification was about 100 °C lower than that for 10 vol.% $ZrSi_2$ (ZSZ10). The relative density exceeding 85% was obtained at 1400 °C for 30 min under a pressure of 30 MPa for the four compositions. This indicated that most of the densification occurred at the first stage of sintering. The density

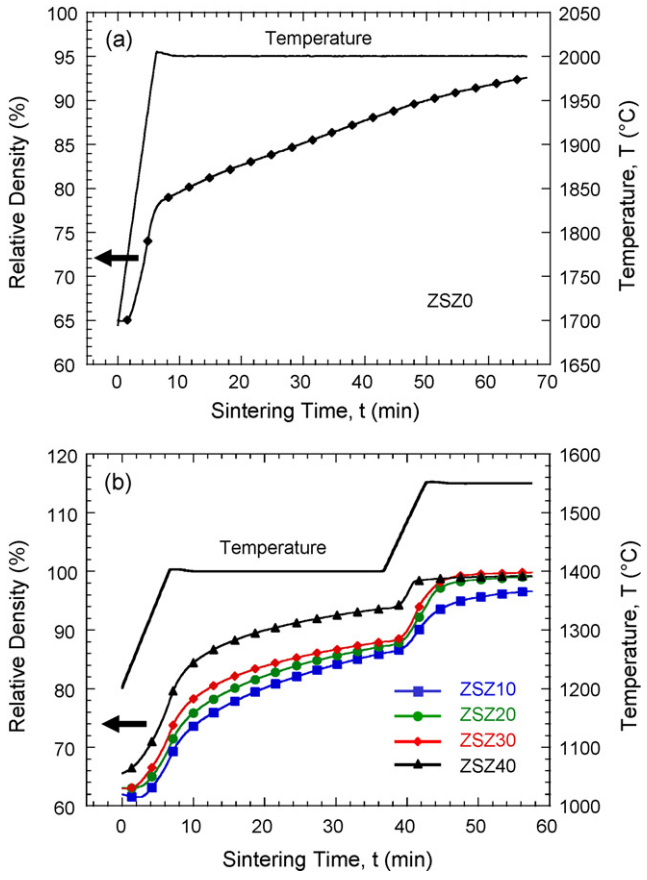

Fig. 1. Typical examples of shrinkage curves obtained during hot-pressing cycle for (a) single-phase ZrB_2 ceramic and (b) ZrB_2–$ZrSi_2$ composites.

exceeding 99% was then obtained at 1550 °C for 15 min for the ZSZ20, ZSZ30, and ZSZ40 powders, i.e., the fully dense ZrB_2–$ZrSi_2$ composites were obtained after the second state of sintering. For ZSZ10 powder, however, the density of 96.6% was obtained after the second state of sintering. The measured true densities and relative densities for the resulting ZrB_2-based composite with $ZrSi_2$ are summarized in Table 1. It is evident that the sinterability of ZrB_2 ceramics is improved by $ZrSi_2$ addition. This means that the fully dense ZrB_2-based ceramics with $ZrSi_2$ may be hot pressed at a temperature below 1600 °C even the 10 vol.% $ZrSi_2$. This indicated that $ZrSi_2$ is an effective additive for lowering the densification temperature of ZrB_2 ceramic.

It is well known that densification of single-phase ZrB_2 powder generally requires very high temperatures (>2100 °C),[6] owing to the covalent character of the bonding as well as to low volume and grain boundary diffusion rates.[20] In addition, oxygen impurities (B_2O_3 and ZrO_2) present in the starting powder have been shown to promote grain growth and inhibit densification in non-oxide ceramic systems such as ZrB_2.[20] In the present study, it is found that $ZrSi_2$ addition improved significantly the sinterability of ZrB_2 ceramic. Obviously, this finding showed that $ZrSi_2$ plays an important role for improving sinterability of single-phase ZrB_2 powder.

It is common that the SiO_2 and B_2O_3 films, respectively, are present on the surfaces of the starting $ZrSi_2$ and ZrB_2 powder

particles. A previous study[21] in TiB_2 showed that the presence of B_2O_3 inhibited densification of TiB_2 due to evaporation of B_2O_3. Therefore, to improve sinterability of ZrB_2, it is necessary to reduce the oxygen content or prevent evaporation of B_2O_3. According to the B_2O_3–SiO_2 phase diagram,[22] it is known that the liquid phase with high viscosity formed when B_2O_3 and SiO_2 are coexisted and the onset temperature of the liquid phase increased with SiO_2 content. Thus, the presence of SiO_2 prevented the evaporation of B_2O_3 during sintering and led to formation of a stable liquid phase between grains, in turn result in improvement of densification. The improvement is enhanced with amount of intergranular liquid phase. In this study, the shrinkage curves obtained during hot-pressing cycle showed the onset temperature of densification lowered with $ZrSi_2$ content (Fig. 1(b)), as a result of the increase of intergranular liquid phase. Improvement of densification due to the presence of intergranular liquid phase is documented in the literature. Sciti et al.[23] showed that the addition of $MoSi_2$ significantly improved densification of HfB_2 powders, as a result of the presence of intergranular liquid phase. They concluded that the presence of intergranular liquid phase favors the process of grain rearrangement as well as improves the packing density of particles, and removes the oxide species from the surface of HfB_2 particles. For the ZrB_2–$ZrSi_2$ materials investigated in this study, two major causes could be considered for the improvement of densification of ZrB_2 powders due to addition of $ZrSi_2$. One is a formation of intergranular liquid phase between $ZrSi_2$ and ZrB_2 particles due to interaction of oxides that presented on the surfaces of particles. Another cause is ductile deformation of $ZrSi_2$ particles at high temperature (>800 °C).[24] This deformation could lead to forcing soft $ZrSi_2$ particles to fill in the voids left by the ZrB_2 skeleton under pressure during sintering, in turn result in improvement of densification.

3.2. Microstructure

In Fig. 2, typical examples of X-ray diffraction patterns for the various hot-pressed ZrB_2–$ZrSi_2$ composites are presented. From this figure, it is found that the ZrB_2 and $ZrSi_2$ phases are primary crystalline phases and the trace amount of ZrO_2 and SiC phases are also present for all the compositions. The trace of ZrO_2 should be attributed to both oxygen contamination of the starting ZrB_2 powder and to oxygen take-up during the milling procedure. The presence of SiC phase should be associated with C contamination of the starting $ZrSi_2$ powder as well as with SiC contamination of media during the milling procedure.

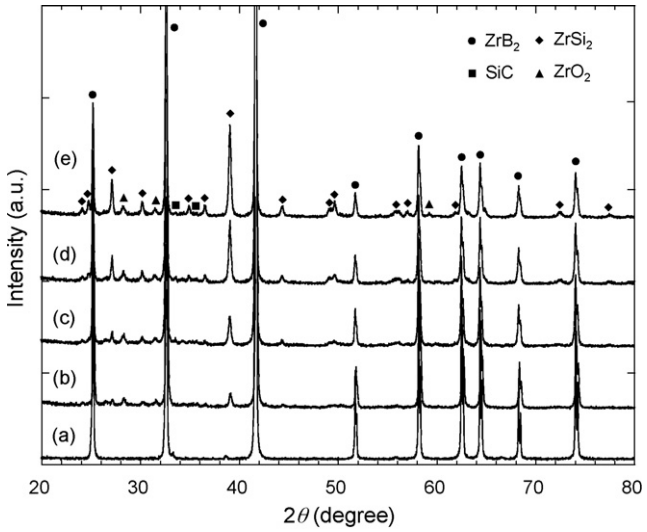

Fig. 2. X-ray diffraction patterns for the various hot-pressed ZrB_2–$ZrSi_2$ composites: (a) ZSZ0, (b) ZSZ10, (c) ZSZ20, (d) ZSZ30, and (e) ZSZ40.

Microstructure of the hot-pressed single-phase ZrB_2 ceramic and ZrB_2–$ZrSi_2$ composites is observed under backscattered electron FE-SEM imaging, typical examples are shown in Fig. 3. In order to compare the effect of two-step sintering on the microstructure, the ZrB_2-containing 20 vol.% $ZrSi_2$ (ZSZ20) sintered at 1550 °C without the intermediate step at 1400 °C was also observed under SEM, which example is shown in Fig. 3(f). For the single-phase ZrB_2 ceramic, the equiaxed ZrB_2 grains are observed. Many pores located at multiple grains junctions, and some pores are present at two ZrB_2 grains boundaries. For the ZrB_2–$ZrSi_2$ composites, on the other hand, the general microstructures are similar for four compositions, consisting of the equiaxed ZrB_2 grains (brighter contrast), the irregular $ZrSi_2$ grains (dark contrast), and ZrO_2 grains (white contrast). EDX analysis identified that the light-gray phase and the intermediate-gray phase (brighter contrast) in the backscattered electron FE-SEM images are ZrB_2 phase, and the phase with the darkest contrast is $ZrSi_2$ phase with oxygen and boron contaminations. These contaminations result from starting $ZrSi_2$ and ZrB_2 powders and they should be formed an intergranular amorphous phase during sintering. Hwang et al.[25] showed the presence of the intergranular amorphous phase in the hot-pressed ZrB_2-based composites with nano-sized SiC addition, as a result of the interaction of impurities of the intergranular amorphous phase in hot-pressed ZrB_2-based composites with nano-SiC addition, as a result of the interaction of impurities. Although the amorphous

Table 2
Shear modulus, Young's modulus, bulk modulus, Poisson's ratio, fracture toughness and flexural strength measured for the various hot-pressed ZrB_2–$ZrSi_2$ composites

Materials	Elastic properties				Fracture toughness, K_{IC} (MPa m$^{1/2}$)	4-Point flexural strength, σ_{FS} (MPa)
	G (GPa)	E (GPa)	B (GPa)	V		
ZSZ0	185	417	185	0.15	4.8 ± 0.4	457 ± 58
ZSZ10	187	432	211	0.16	3.8 ± 0.3	483 ± 22
ZSZ20	192	445	217	0.16	4.4 ± 0.5	556 ± 54
ZSZ30	182	427	221	0.18	4.4 ± 0.2	555 ± 42
ZSZ40	168	397	205	0.18	3.9 ± 0.4	382 ± 78

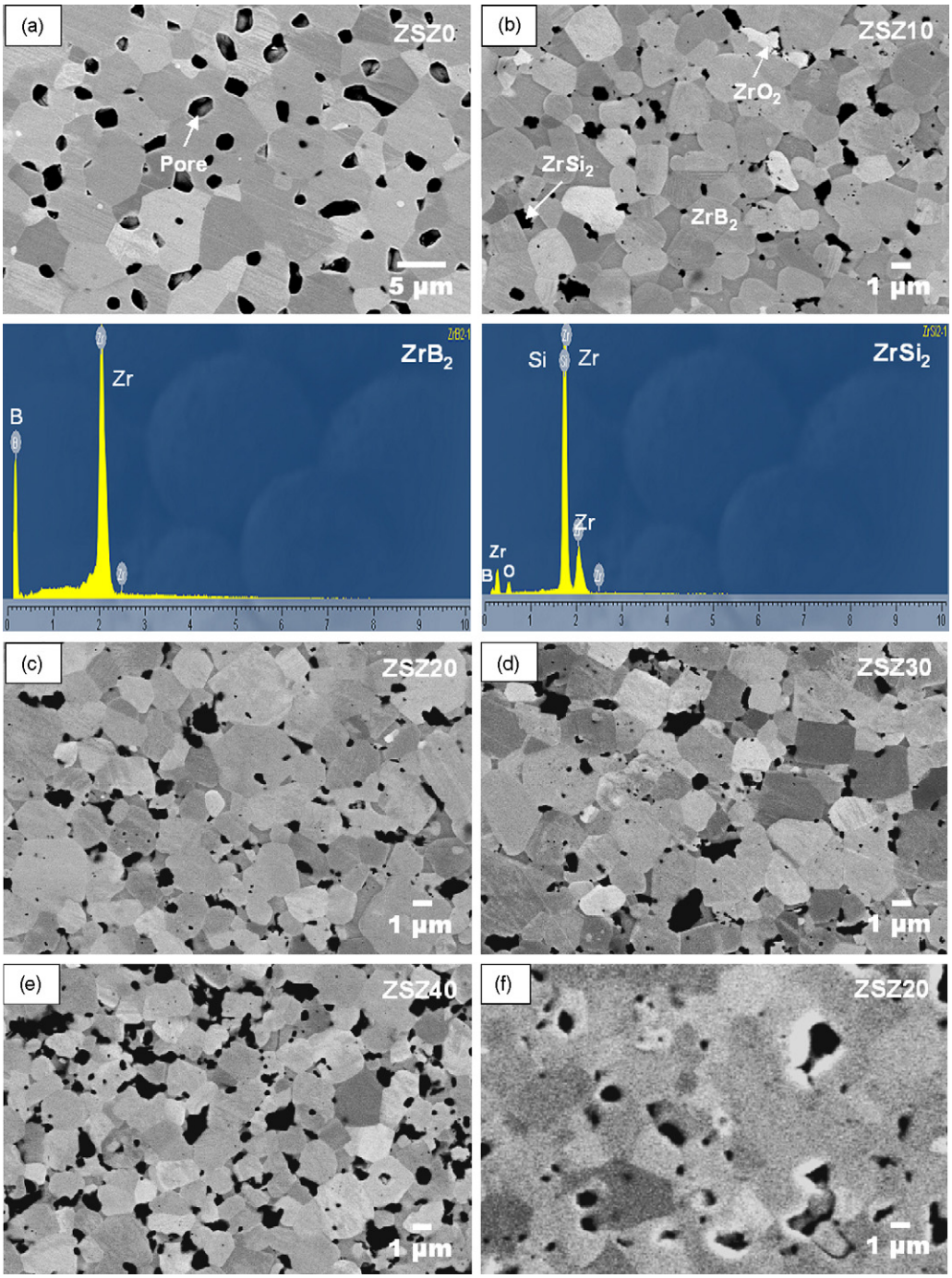

Fig. 3. Typical examples of backscattered electron FE-SEM images for the various hot-pressed ZrB_2–$ZrSi_2$ composites: (a) ZSZ0, (b) ZSZ10, (c) ZSZ20, (d) ZSZ30, (e) ZSZ40, and (f) ZSZ20 consolidated at 1550 °C without the intermediate step 1400 °C.

phase is too thin to distinguish under SEM, similar intergranular phase is expected in the ZrB_2–$ZrSi_2$ composites investigated in this study, as a result of interaction of SiO_2, ZrO_2 and B_2O_3 presented on the starting $ZrSi_2$ and ZrB_2 powders.

Moreover, it is found that the ZrB_2 grains were fine and homogeneous in the microstructure of the two-step sintering composites compared with the single-phase ZrB_2 (Fig. 3(a)) as well as with the ZrB_2–$ZrSi_2$ composites sintered at 1550 °C without the intermediate step at 1400 °C (Fig. 3(f)). The grain sizes of ZrB_2 and $ZrSi_2$ measured in the various hot-pressed ZrB_2-based ceramics with $ZrSi_2$ are also summarized in Table 1. For the single-phase ZrB_2, the ZrB_2 grain was significantly coarsened during sintering. For the ZrB_2–$ZrSi_2$ compositions, however, the ZrB_2 grains sizes are almost constant in two-step sintering composites for four compositions, regardless of $ZrSi_2$ content. On contrary, the ZrB_2 grain was coarsened in the ZSZ20 consolidated at 1550 °C, and ZrB_2 grain size is larger by a factor of ~2 than the two-step sintering ZSZ20. Obviously, the fine microstructure may be attributed to the two-step sintering process used which consists of a first stage at lower temper-

ature for longer time and a second one at higher temperature for short time. This advantage of such a cycle is that most of the densification occurs at a rather low temperature and that the higher temperature stage is short. Therefore, there is no time for grain growth to occur, and the resulting microstructure is fine and homogeneous. In contrary, the $ZrSi_2$ grains were inhomogeneous and had a bimodal grain size distribution. Some $ZrSi_2$ grains were very fine (<0.2 μm) and they were present at two ZrB_2 grains boundaries and/or within ZrB_2 grains. Some $ZrSi_2$ grains were considerably coarse and irregular (~3 μm). The coarse round $ZrSi_2$ grains located at multiple ZrB_2 grains junctions and the irregular $ZrSi_2$ grains were present at two ZrB_2 grains boundaries (Fig. 3(b)–(e)). Similar morphologies of $ZrSi_2$ were also observed in the ZSZ20 consolidated at 1550 °C without the intermediate step at 1400 °C. The different morphologies of $ZrSi_2$ grains may be associated with the ductile deformation of soft $ZrSi_2$ phase during hot pressing. The soft $ZrSi_2$ powder particles located between the ZrB_2 particles were rolled by the rigid ZrB_2 particles under a pressure during sintering. This thinning process will result in following two possible moving ways of $ZrSi_2$ particles: (i) $ZrSi_2$ particles are removed from two ZrB_2 grains and filled in the voids left by the multiple ZrB_2 grains skeleton, forming some coarse $ZrSi_2$ grains at the multiple grains junctions; and (ii) $ZrSi_2$ particles are rolled into a thin layer between two ZrB_2 grains and/or are broken into some fine particles because rough surface of the rigid ZrB_2 powder particles. This process should continue until the densification is reached. In addition, although the significant difference in the morphology of $ZrSi_2$ grains was not observed in the FEM-SEM images for the four material compositions, the $ZrSi_2$ grains tend to coarsen with $ZrSi_2$ content (Table 1). In particular for ZSZ40 composition, the coarse $ZrSi_2$ grains significantly increased, and several $ZrSi_2$ particles combined together for forming some $ZrSi_2$ particles agglomerates.

3.3. Mechanical properties

Shear modulus, Young's modulus, bulk modulus, Poisson's ratio, fracture toughness and room temperature flexural strength measured in the various hot-pressed ZrB_2–$ZrSi_2$ composites are summarized in Table 2. From this table, it is found that the shear modulus, Young's modulus, and bulk modulus are lower for single-phase ZrB_2 ceramic than for ZrB_2-based ceramics with $ZrSi_2$ due to the presence of pores in the former (Table 1). Also, it is found that these moduli lowered with increasing $ZrSi_2$ content. For ZSZ40, in particular, the shear modulus, Young's modulus and bulk modulus dropped 168, 397, and 205 GPa from 192, 445, and 217 GPa for ZSZ20, respectively, for approximate loss of ~13%, ~11%, and ~6%. One exception for the lower shear modulus, Young's modulus, and bulk modulus for ZSZ10 than those of ZSZ20 and ZSZ30, was a result of the presence of pores (~4 vol.%) because the porosity led to the decreases of the moduli.[18] In addition, Young's modulus measured in the ZrB_2–$ZrSi_2$ composites was lower than the reported values for single-phase ZrB_2 ceramic (>500 GPa).[26,27] The decreases of the moduli due to $ZrSi_2$ addition may be attributed to lower moduli of $ZrSi_2$ than that of ZrB_2.[24,26,27] In contrast, Poisson's ratio remains almost constant for four composition materials, regardless of $ZrSi_2$ content, and the value is similar to that of single-phase ZrB_2 ceramic. This suggests that Poisson's ratio is insensitive to $ZrSi_2$ addition as well as to added content. Also, fracture toughness measured in the ZrB_2–$ZrSi_2$ composites showed a compositional dependence, and it decreased with increasing $ZrSi_2$ content. One exception is lower fracture toughness for 10 vol.% $ZrSi_2$-containing ZrB_2 (ZSZ10). The range of fracture toughness values was measured to be 3.8–4.8 MPa $m^{1/2}$.

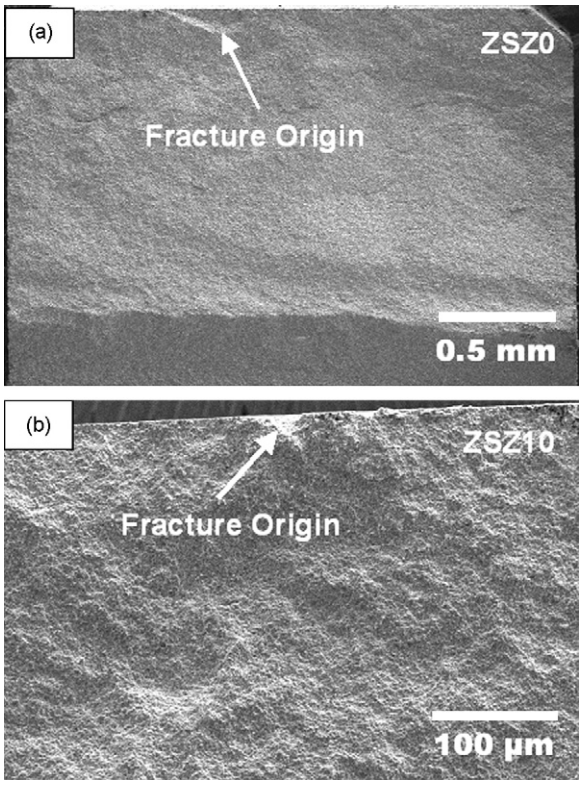

Fig. 4. Macro-fracture appearance of fracture surfaces for the various hot-pressed ZrB_2–$ZrSi_2$ composites: (a) ZSZ0 and (b) ZSZ10.

Moreover, it is found that the flexural strengths of the composites were almost constant for $ZrSi_2$ content of 30 vol.% or less (Table 2). The flexural strength measured was significantly higher than that reported for single-phase ZrB_2 ceramic,[1] but it was lower than the value reported in the hot-pressed 15 vol.% $MoSi_2$-containing ZrB_2 composite.[10] One exception was a relatively low-room temperature flexural strength measured for ZSZ10, as a result of the presence of pores (~4 vol.%, Table 1). For ZSZ40, however, the flexural strength measured dropped from 556 MPa for ZSZ-20 to 382 MPa, for approximate loss of ~30%. In addition, although the average strength remains constant with $ZrSi_2$ content for $ZrSi_2$ content of 30 vol.% or less, the strength scattering increased with $ZrSi_2$ content.

In Fig. 4, the macro-appearance of fracture surface of the hot-pressed ZrB_2–$ZrSi_2$ composites is presented. It is evident that the fracture origin was located at and/or near the surface. The major cause of failure presumably was the presence of defects, e.g., pores, at and/or near the surface. In addition, the fracture surface of the composites was examined under high-magnification FE-SEM, typical examples are shown in Fig. 5.

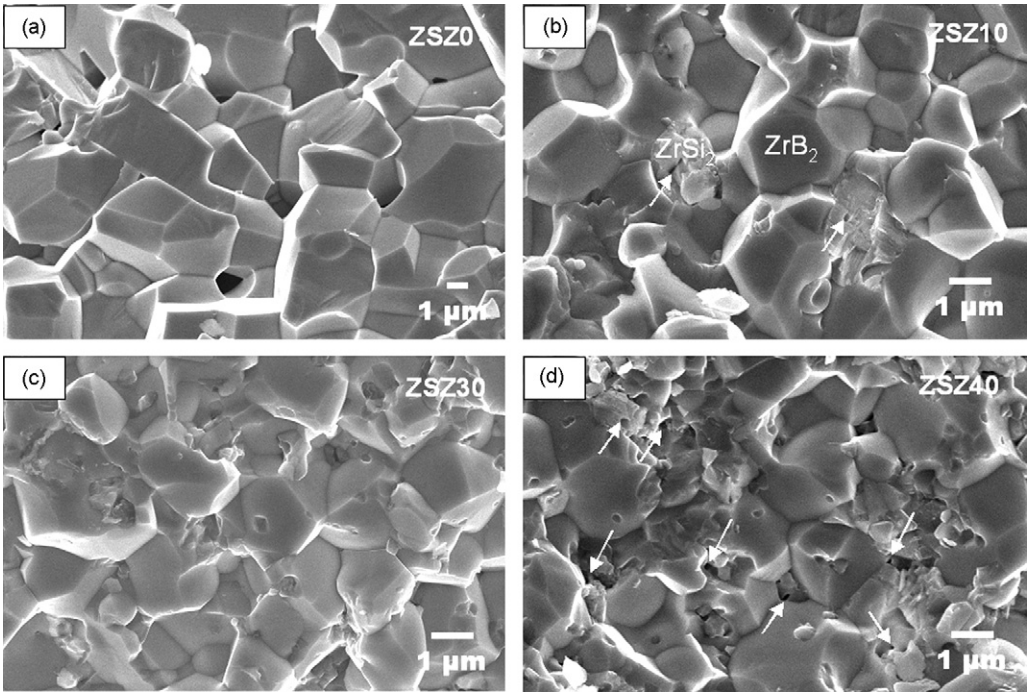

Fig. 5. Typical FE-SEM images of fracture surfaces for the various hot-pressed ZrB_2–$ZrSi_2$ composites: (a) ZSZ0, (b) ZSZ10, (c) ZSZ30, and (d) ZSZ40.

For a single-phase ZrB_2 ceramic (Fig. 5(a), typical intergranular fracture is observed. The intergranular fracture fashion led to a higher fracture toughness of single-phase ZrB_2 (Table 2). For the ZrB_2–$ZrSi_2$ composites (Figs. 5(b)–5(d)), the ZrB_2 phase still shows a typical intergranular fracture, whereas the $ZrSi_2$ phase shows a different fracture fashion: intragranular fracture. Although the fracture surfaces of these compositions are relatively flat and many intergranular fracture characterizations, ZSZ40 composition showed a much more transgranular character (Fig. 5(d)). In addition, it is found that the pores were presented within $ZrSi_2$ (indicated by arrows in Fig. 5(b)). In particular, for ZSZ40 composition material, some pores were observed within large $ZrSi_2$ agglomerates as well as between the ZrB_2 grains (indicated by arrows in Fig. 5(d)). Presumably, the presence of the large $ZrSi_2$ agglomerates containing pores is responsible for the lowered flexural strength and the increase in strength scattering observed in the ZSZ40 composite, compared to other compositions materials.

4. Conclusions remarks

(1) The $ZrSi_2$ significantly lowered the onset temperature of densification of ZrB_2 ceramics. The onset temperature of densification lowered with $ZrSi_2$ content, and the temperature was in the range from ∼1180 to ∼1280 °C. The ZrB_2-based composites with 20–40 vol.% $ZrSi_2$ hot pressed at 1550 °C were fully dense (relative density>99%).

(2) The microstructure of the resulting ZrB_2–$ZrSi_2$ composites consisted of the equiaxed ZrB_2 grains and the irregular $ZrSi_2$ grains. The ZrB_2 grains were fine and homogenous, while the $ZrSi_2$ grains had a bimodal grain distribution.

(3) The shear modulus, Young's modulus, and bulk modulus of the composites lowered with $ZrSi_2$ content. The shear modulus was in the range of 168 and 192 GPa, while Young's modulus is in the range of 397 and 445 GPa and the bulk modulus is in the range of 205 and 221 GPa. The range of fracture toughness values was measured to be 3.8–4.8 MPa $m^{1/2}$, dependent on $ZrSi_2$ content. On the other hand, the room temperature flexural strength of the ZrB_2–$ZrSi_2$ composites was almost constant for $ZrSi_2$ content ranging from 20 to 30 vol.%. For 40 vol.% $ZrSi_2$, however, the strength significantly lowered.

References

1. Kuwabara, K., Some characteristics and applications of ZrB_2 ceramics. *Bull. Ceram. Soc. Jpn.*, 2002, **37**(4), 267–271.
2. Upadhya, K., Yang, J.-M. and Hoffmann, W. P., Materials for ultrahigh temperature structural applications. *Am. Ceram. Soc. Bull.*, 1997, **76**(12), 51–56.
3. Brown, A. S., Hypersonic designs with a sharp edge. *Aerospace Am.*, 1997, **35**(9), 20–21.
4. Mroz, C., Zirconium diboride. *Am. Ceram. Soc. Bull.*, 1994, **73**(6), 141–142.
5. Norasetthekul, S., Eubank, P. T., Bradley, W. L., Bozkurt, B. and Stucker, B., Use of zirconium diboride-copper as an electrode in plasma applications. *J. Mater. Sci.*, 1999, **34**(6), 1261–1270.
6. Pastor, M., Metallic borides: preparation of solid bodies. In *Sintering Methods and Properties of Solid Bodies; Boron and Refractory Borides*, ed. V. I. Matkovich. Springer, New York, 1977, pp. 457–493.
7. Monteverde, F. and Bellosi, A., Effect of the addition of silicon nitride on sintering behavior and microstructure of zirconium diboride. *Scr. Mater.*, 2002, **46**, 223–228.
8. Monteverde, F. and Bellosi, A., Development and characterization of metal-diboride-based composites toughened with ultra-fine SiC particulates. *Solid State Sci.*, 2005, **7**, 622–630.

9. Monteverde, F. and Bellosi, A., Beneficial effects of AlN as sintering aid on microstructure and mechanical properties of hot-pressed ZrB_2. *Adv. Eng. Mater.*, 2003, **5**, 508–512.
10. Bellosi, A., Monteverde, F. and Sciti, D., Fast densification of ultra-high-temperature ceramics by spark plasma sintering. *Int. J. Appl. Ceram. Technol.*, 2006, **3**(1), 32–40.
11. Sciti, D., Guicciardi, S., Bellosi, A. and Pezzotti, G., Properties of a pressureless-sintered ZrB_2–$MoSi_2$ ceramic composites. *J. Am. Ceram. Soc.*, 2006, **89**(7), 2320–2322.
12. Sciti, D., Brach, M. and Bellosi, A., Oxidation behavior of a pressureless sintered ZrB_2–$MoSi_2$ ceramic composites. *J. Mater. Res.*, 2005, **20**(4), 922–930.
13. Guo, S. Q., Nishimura, T., Kagawa, Y. and Tanaka, H., Thermal and electric properties in hot-pressed ZrB_2–$MoSi_2$–SiC composites. *J. Am. Ceram. Soc.*, 2007, **90**(7), 2255–2258.
14. Ondik, H. M. and McMurdie, H. F., Phase Diagram for Zirconium + Zirconia Systems, The American Ceramics Society, 735 Ceramic Place, Westerville, Ohio 43081, USA, 1998.
15. Jeng, Y.-L. and Lavernia, E. J., Processing of molybdenum disilicide. *J. Mater. Sci.*, 1994, **29**, 2557–2571.
16. de Mestral, F. and Thevenot, F., Ceramic composites: TiB_2–TiC–SiC. *J. Mater. Sci.*, 1991, **26**, 5547–5560.
17. Mendelson, M. I., Average grain size in polycrystalline ceramics. *J. Am. Ceram. Soc.*, 1969, **52**(8), 443–446.
18. Guo, S. Q., Hirosaki, N., Yamamoto, Y., Nishimura, T. and Mitomo, M., Hot-press sintering silicon nitride with Lu_2O_3 addition: elastic moduli and fracture toughness. *J. Eur. Ceram. Soc.*, 2003, **23**, 537–545.
19. Anstis, G. R., Chantikul, P., Lawn, B. R. and Marshall, D. B., A critical evaluation of indentation techniques for measuring fracture toughness. I. Direct crack measurements. *J. Am. Ceram. Soc.*, 1981, **64**(9), 533–538.
20. Telle, R., Sigl, L. S. and Takagi, K., Boride-based hard materials. In *Handbook of Ceramic Hard Materials*, *vol. 2*, ed. R. Riedel. Wiley-VCH, Weinheim, Germany, 2000, pp. 802–945.
21. Baik, S. and Becher, P. F., Effect of oxygen contamination on densification of TiB_2. *J. Am. Ceram. Soc.*, 1987, **70**(8), 527–530.
22. Rockett, T. J. and Foster, W. R., Phase relations in the system boron oxide-silica. *J. Am. Ceram. Soc.*, 1965, **48**(2), 75–80.
23. Sciti, D., Silvestroni, L. and Bellosi, A., Fabrication and properties of HfB_2–$MoSi_2$ composites produced by hot pressing and spark plasma sintering. *J. Mater. Res.*, 2006, **21**(6), 1460–1466.
24. Rosenkranz, R. and Frommeyer, G., Microstructures and properties of the refractory compounds $TiSi_2$ and $ZrSi_2$. *Z. Metallkd.*, 1992, **83**(9), 685–689.
25. Hwang, S. S., Vasiliev, A. L. and Padture, N. P., Improved processing and oxidation-resistance of ZrB_2 ultra-high temperature ceramics containing SiC nanodispersoids. *Mater. Sci. Eng.*, 2007, **A464**, 216–224.
26. Holleck, H., Material selection for hard coatings. *J. Vac. Sci. Technol.*, 1986, **4**, 2661–2669.
27. Chamberlain, A. L., Farenholtz, W. G. and Hilmas, G. E., High-strength zirconium diboride-based ceramics. *J. Am. Ceram. Soc.*, 2004, **87**(6), 1170–1172.